10-1-1996

Dimer and Néel order-parameter fluctuations in the spin-fluid phase of the s=1/2 spin chain with first- and second-neighbor couplings

Yongmin Yu
University of Rhode Island

Gerhard Müller
University of Rhode Island, gmuller@uri.edu

V. S. Viswanath
University of Rhode Island

Citation/Publisher Attribution

Yongmin Yu, Gerhard Müller, and V.S. Viswanath. *Dimer and Néel order-parameter fluctuations in the spin-fluid phase of the s=1/2 spin chain with first and second neighbor couplings.* Phys. Rev. B **54** (1996), 9242-9249.
Available at: http://dx.doi.org/10.1103/PhysRevB.54.9242

Dimer and Néel order-parameter fluctuations in the spin-fluid phase of the s=1/2 spin chain with first- and second-neighbor couplings

Dimer and Néel order-parameter fluctuations in the spin-fluid phase of the $s=\frac{1}{2}$ spin chain with first- and second-neighbor couplings

Yongmin Yu and Gerhard Müller
Department of Physics, The University of Rhode Island, Kingston, Rhode Island 02881-0817

V. S. Viswanath
Solid State Division, Oak Ridge National Laboratory, Oak Ridge, Tennessee 37831-6032

(Received 9 April 1996)

The dynamical properties at $T=0$ of the one-dimensional (1D) $s=\frac{1}{2}$ nearest-neighbor (NN) XXZ model with an additional isotropic next-nearest-neighbor (NNN) coupling are investigated by means of the recursion method in combination with a weak-coupling continued-fraction analysis. The focus is on the dynamic structure factors $S_{zz}(q,\omega)$ and $S_{DD}(q,\omega)$, which describe (for $q=\pi$) the fluctuations of the Néel and dimer order parameters, respectively. We calculate the dependence on the exchange constants of the infrared exponent, the renormalized bandwidth of spinon excitations, and the spectral-weight distribution in $S_{zz}(\pi,\omega)$ and $S_{DD}(\pi,\omega)$, all in the spin-fluid phase, which is realized for planar NN anisotropy and sufficiently weak NNN coupling. For some parameter values we find a discrete branch of excitations above the spinon continuum. They contribute to $S_{zz}(q,\omega)$ but not to $S_{DD}(q,\omega)$. [S0163-1829(96)02538-6]

I. INTRODUCTION

Quantum many-body systems with competing interactions are apt to exhibit ordering tendencies in the ground state of which no trace exists in the presence of any one coupling alone and which are impossible to predict on the basis of a classical model with both couplings. Among the many different model systems where this phenomenon is manifest, the Heisenberg antiferromagnet with nearest-neighbor (NN) and next-nearest-neighbor (NNN) couplings on a bipartite lattice is a prominent example. For coupling strengths of comparable magnitude on the square lattice, various ordering tendencies including Néel order, collinear order, dimer order, twist order, and chiral order are in competition with each other and with disordering tendencies such as embodied by the resonating valence-bond state.[1]

The one-dimensional (1D) version of this model had gained prominence many years before, when the ground state for one particular ratio of the coupling constants was found to be a pure dimer state.[2,3] Spontaneous dimerization is a true quantum phenomenon. Several studies have succeeded in mapping out the zero-temperature phase diagram of this model in one or the other extended parameter space,[4–7] albeit with little emphasis on dynamical properties. In this paper we study the $T=0$ dynamics of the Hamiltonian

$$H=\sum_{l=1}^{N}\{J_\perp[S_l^xS_{l+1}^x+S_l^yS_{l+1}^y]+J_zS_l^zS_{l+1}^z+J_2\mathbf{S}_l\cdot\mathbf{S}_{l+2}\}, \tag{1.1}$$

parametrized by the two coupling constants $\Delta=J_z/J_\perp$ and $\Lambda=J_2/J_\perp$. Extending the parameter space to cases with uniaxial anisotropy in the NN coupling offers the advantage that the model with $\Delta=\Lambda=0$, which reduces to a system of free lattice fermions,[8,9] can be used as a convenient starting point for weak-coupling approaches.

A schematic representation of the $T=0$ phase diagram is shown in Fig. 1. The free-fermion point ($\Delta=0,\ \Lambda=0$) is located in the middle of the spin-fluid phase. Here the system is a Luttinger liquid. The ground state is critical—i.e., the excitation spectrum is gapless—and the static spin and dimer correlation functions decay algebraically with exponents depending on the coupling constants of the two types of interaction.

For $\Lambda<0$ the NNN coupling strengthens the correlations produced by the NN coupling and thus reinforces the prevailing ordering tendency. Therefore, we expect to find ferromagnetic long-range order in the region ($\Lambda\leqslant 0,\ \Delta\leqslant -1$) and antiferromagnetic long-range order in the region ($\Lambda\leqslant 0,\ \Delta>1$). For $-1<\Delta\leqslant 1$ the NN interaction alone is known not to support any kind of long-range order. No phase transition is suspected to occur if a negative NNN coupling is added.

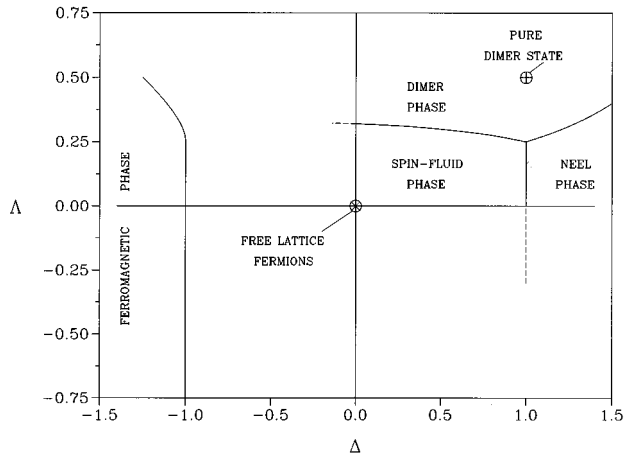

FIG. 1. Zero-temperature phase diagram of the model system (1.1) with coupling constants $\Delta=J_z/J_\perp$ and $\Lambda=J_2/J_\perp$ in a schematic representation.

For $\Lambda>0$ the NN and NNN couplings are in competition with each other. The latter thus frustrates the ordering tendency of the former. One predictable consequence is that the boundary of the ferromagnetic phase, which is located at $\Delta=-1$ for $\Lambda<1/4$, bends to the left in Fig. 1 for increasing NNN coupling.[10] Increasing amounts of uniaxial anisotropy are necessary to stabilize the spin alignment. A simple spin-wave stability criterion yields the expression $1/\Lambda=4[|\Delta|-\sqrt{\Delta^2-1}]$ for the phase boundary in that region.

In the region of planar anisotropy, $|\Delta|<1$, the interplay of the two competing forces in the presence of quantum fluctuations produces the dimer phase. Curiously, within the dimer phase there exists one point in parameter space, $(\Delta=1,\ \Lambda=1/2)$,[2,3] where the ground state is a pure dimer state with no correlated fluctuations, notwithstanding the fact that this phase owes its very existence to quantum fluctuations. However, the $T=0$ dynamics at this point turns out to be only marginally simpler than elsewhere in the dimer phase, where the structure of the ground state is much more complex.[11]

In the region of uniaxial antiferromagnetic anisotropy, $\Delta>1$, there exists a Néel phase. Like the ferromagnetic phase, it is destabilized by sufficiently strong competing NNN coupling. The phase boundaries between the spin-fluid, dimer, and Néel phases as sketched in Fig. 1 were first proposed by Haldane[5] based on a continuum fermion theory. The impact of the transitions between the Néel, dimer, and spin-fluid phases on the $T=0$ dynamics will be explored in a separate study.[12]

II. SPIN AND DIMER FLUCTUATIONS

The Néel order parameter (staggered magnetization) and the dimer order parameter for the model system (1.1) are given, respectively, by the operators

$$\overline{M_z}=\frac{1}{N}\sum_{l=1}^{N}(-1)^l S_l^z, \tag{2.1}$$

$$D=\frac{1}{N}\sum_{l=1}^{N}(-1)^l D_l, \quad D_l=S_l^+S_{l+1}^-+S_l^-S_{l+1}^+. \tag{2.2}$$

Néel order in its purest form is realized in the states

$$|\Phi_1^z\rangle=|\uparrow\downarrow\uparrow\cdots\downarrow\rangle, \quad |\Phi_2^z\rangle=|\downarrow\uparrow\downarrow\cdots\uparrow\rangle, \tag{2.3}$$

and pure dimer order in the states

$$|\Phi_1^D\rangle=[1,2][3,4]\cdots[N-1,N], |\Phi_2^D\rangle=[2,3][4,5]\cdots[N,1], \tag{2.4}$$

where the singlets $[l,l+1]=\{|\uparrow\downarrow\rangle-|\downarrow\uparrow\rangle\}/\sqrt{2}$ are formed by pairs of NN spins. In the ground state of Eq. (1.1), the former is realized at $(\Lambda=0,\ \Delta=\infty)$ and the latter at $(\Lambda=1/2,\ \Delta=1)$.

Néel ordering manifests itself in the two-spin correlation function $\langle S_l^z S_{l+n}^z\rangle$ and dimer ordering in the four-spin correlation function $\langle D_l D_{l+n}\rangle$. For translationally invariant and orthonormal linear combinations of the symmetry-breaking Néel states (2.3) and dimer states (2.4), they are $\langle S_l^z S_{l+n}^z\rangle=\frac{1}{4}(-1)^n$, $\langle D_l D_{l+n}\rangle=0$ $(n\neq 0)$ and $\langle S_l^z S_{l+n}^z\rangle=0$ $(|n|\neq 1)$, $\langle D_l D_{l+n}\rangle-\langle D_l\rangle\langle D_{l+n}\rangle=\frac{1}{4}(-1)^n$ $(n\neq 0)$, respectively, and reflect the long-range nature of the two types of ordering. In the free-fermion ground state at $\Delta=\Lambda=0$, by contrast, the same correlation functions decay algebraically,[8]

$$\langle S_l^z S_{l+n}^z\rangle=\frac{1}{2\pi^2 n^2}[\cos(n\pi)-1], \tag{2.5}$$

$$\langle D_l D_{l+n}\rangle-\langle D_l\rangle\langle D_{l+n}\rangle=\frac{1}{\pi^2 n^2}\left[\frac{2n^2-1}{n^2-1}\cos(n\pi)+\frac{1}{n^2-1}\right]. \tag{2.6}$$

In this study we use the recursion method[13,14] to investigate the dynamical (i.e., frequency-dependent) order-parameter fluctuations as probed by the dynamic spin structure factor $S_{zz}(q,\omega)$ and the dynamic dimer structure factor $S_{DD}(q,\omega)$, i.e., by the function

$$S_{AA}(q,\omega)=\int_{-\infty}^{+\infty}dt e^{i\omega t}\langle A_q^\dagger(t)A_q\rangle, \tag{2.7}$$

where A_q stands for the spin and dimer fluctuation operators,

$$S_q^z=N^{-1/2}\sum_l e^{iql}S_l^z, \quad D_q=N^{-1/2}\sum_l e^{iql}[D_l-\langle D_l\rangle]. \tag{2.8}$$

For the calculation of the dynamic correlation function $\langle\Phi|A_q^\dagger(t)A_q|\Phi\rangle$ in the ground state $|\Phi\rangle$ of the system, it can be based on an orthogonal expansion of the dynamical variable $A_q(t)$ (Liouvillian representation[15]) or on an orthogonal expansion of the wave function $A_q(-t)|\Phi\rangle$ (Hamiltonian representation[16]). The algorithms of both representations, which have been described and illustrated in a recent monograph,[17] produce equivalent data. These data are expressible most concisely in terms of a sequence of continued-fraction coefficients $\Delta_1^A(q)$, $\Delta_2^A(q)$, . . . for the relaxation function

$$c_0^{AA}(q,z)=\cfrac{1}{z+\cfrac{\Delta_1^A(q)}{z+\cfrac{\Delta_2^A(q)}{z+\ \ldots}}}, \tag{2.9}$$

which is the Laplace transform of the symmetrized and normalized correlation function $\mathrm{Re}\langle\Phi|A_q^\dagger(t)A_q|\Phi\rangle/\langle\Phi|A_q^\dagger A_q|\Phi\rangle$. The $T=0$ dynamic structure factor (2.7) is then obtained from Eq. (2.9) via

$$S_{AA}(q,\omega)=4S_{AA}(q)\Theta(\omega)\lim_{\epsilon\to 0}\mathrm{Re}[c_0^{AA}(q,\epsilon-i\omega)], \tag{2.10}$$

where $S_{AA}(q)=\langle\Phi|A_q^\dagger A_q|\Phi\rangle$ is the static structure factor (integrated intensity).

For the reconstruction of $S_{AA}(q,\omega)$ based on a number of coefficients $\Delta_k^A(q)$ extracted from the finite-size ground-state wave function $|\Phi\rangle$, we employ techniques of continued-fraction analysis described previously in the context of other applications, one pertaining to the strong-coupling regime[18] and the other to the weak-coupling regime[19] of a given quantum many-body system.

III. RESULTS AND INTERPRETATION

For the special case $\Lambda=\Delta=0$ of the spin model (1.1), dynamic correlation functions can be calculated exactly. The evaluation is particularly simple for the two dynamic structure factors of interest here, because the operators involved, S_q^z and D_q, are density operators in the fermion representation:[20,21]

$$S_{zz}(q,\omega)=\frac{2}{\sqrt{4J_\perp^2\sin^2(q/2)-\omega^2}}, \tag{3.1}$$

$$S_{DD}(q,\omega)=\frac{\sqrt{4J_\perp^2\sin^2(q/2)-\omega^2}}{J_\perp^2\sin^2(q/2)}, \tag{3.2}$$

for $J_\perp|\sin q|<\omega<2J_\perp|\sin(q/2)|$. Both quantities have the same excitation spectrum, the particle-hole continuum of free fermions. For other dynamical variables such as S_q^x the evaluation of dynamic correlation functions is much more involved, and the results have a much more complicated structure with dynamically relevant excitation spectra of unbounded support.[22]

In the XXZ antiferromagnet with planar anisotropy ($\Lambda=0, 0\leqslant\Delta\leqslant 1$), the spectral weight in $S_{zz}(q,\omega)$ is known[23] to be dominated by a continuum of unbound two-spinon states with upper and lower boundaries

$$\epsilon_L(q)=J_\Delta|\sin q|,\quad \epsilon_U(q)=2J_\Delta|\sin(q/2)|, \tag{3.3}$$

where $J_\Delta=\pi J_\perp\sin\vartheta/2\vartheta$, $\cos\vartheta=\Delta$. The Δ dependence of $S_{zz}(q,\omega)$ has already been investigated by several calculational techniques.[19] No equivalent results exist for $S_{zz}(q,\omega)$ in the extended parameter space (Δ,Λ) or for $S_{DD}(q,\omega)$ anywhere in this parameter space. Given the exact solutions (3.1) and (3.2), the case $\Lambda=\Delta=0$ presents itself as a convenient starting point for a weak-coupling continued-fraction analysis of the two dynamic structure factors at $|\Lambda|\ll 1$ and $|\Delta|\ll 1$.[19]

A. Correlation exponent and spin velocity

Haldane's continuum analysis[5] predicts that the exponents which characterize the power-law decay of the spin and dimer correlation functions $\langle S_l^z S_{l+n}^z\rangle\sim(-1)^n n^{-\eta_z}$, $\langle D_l D_{l+n}\rangle-\langle D_l\rangle\langle D_{l+n}\rangle\sim(-1)^n n^{-\eta_D}$, are the same: $\eta_z=\eta_D$. A calculation taking into account both the backscattering and the umklapp terms in the interaction leads to a pair of scaling equations for the dependence of η_z on Δ and Λ. If the umklapp terms are neglected, the analysis yields the explicit result,[5]

$$\eta_z(\Delta,\Lambda)=2\sqrt{(\pi-8\Lambda)/(\pi+4\Delta)}. \tag{3.4}$$

This expression is expected to be most accurate for the special coupling ratio $\Lambda/\Delta=1/6$, where the umklapp terms are absent in the continuum Hamiltonian. Indeed the high accuracy of Eq. (3.4) is demonstrated by the fact that its value $\eta_z=1.006$ at the boundary to the Néel phase ($\Delta=1$, $\Lambda=1/6$) misses the supposedly exact value $\eta_z=1$ by less than 1%. It is not clear how accurate expression (3.4) is for coupling ratios $\Lambda/\Delta\neq 1/6$. At $\Lambda=0$ it can be tested against the exact result[24]

$$\eta_z(\Delta,0)_{\text{exact}}=[1-(1/\pi)\arccos\Delta]^{-1}. \tag{3.5}$$

The two expressions agree to leading order in the coupling constant: $\eta_z=2-4\Delta/\pi+O(\Delta^2)$.

An independent way of determining the correlation exponent η_z for arbitrary coupling ratios Λ/Δ in the region of very weak interaction is provided, as will be demonstrated in Sec. III C, by the weak-coupling continued-fraction analysis of the infrared exponents in the dynamic spin and dimer structure factors,

$$S_{zz}(\pi,\omega)\sim\omega^{\beta_z},\quad S_{DD}(\pi,\omega)\sim\omega^{\beta_D}. \tag{3.6}$$

The continuum analysis suggests that the two infrared exponents are identical and related to η_z:

$$\beta_z=\beta_D=\eta_z-2\,. \tag{3.7}$$

The renormalized spin velocity $v_s(\Delta,\Lambda)$ is another quantity for which the continuum analysis predicts an explicit result,[5]

$$v_s(\Delta,\Lambda)=J_\perp(1+2\Delta/\pi-4\Lambda/\pi). \tag{3.8}$$

It can be checked against the renormalized bandwidth $\omega_0(\Delta,\Lambda)$ of $S_{zz}(\pi,\omega)$ or $S_{DD}(\pi,\omega)$ as obtained (in Sec. III C) via weak-coupling continued-fraction analysis. Both quantities are expected to have the same dependence on the coupling constants except for constant factors. At $\Lambda=0$ we have $\omega_0=\epsilon_U(\pi)=2J_\Delta$ and $v_s=[d\epsilon_U(q)/dq]_{q=0}=J_\Delta$; hence,

$$\omega_0^z=\omega_0^D=2v_s\,. \tag{3.9}$$

B. Weak-coupling continued-fraction coefficients

The exact expressions (3.1) and (3.2) can be recovered for $q=\pi$ from the Δ_k sequences

$$\Delta_k^z(\pi)=J_\perp^2(1+\delta_{k,1}),\quad \Delta_k^D(\pi)=J_\perp^2\,, \tag{3.10}$$

by direct evaluation of Eq. (2.9). These Δ_k values pertain to the infinite system. They are exactly reproduced up to $k=N/2-1$ for $S_{zz}(\pi,\omega)$ and up to $k=N/2-2$ for $S_{DD}(\pi,\omega)$ by the recursion method applied to a chain of N sites with periodic boundary conditions.

Weak coupling ($|\Delta|\ll 1, |\Lambda|\ll 1$) produces systematic deviations of the Δ_k's from the reference sequences (3.10). They are illustrated in the four panels of Fig. 2 for both dynamic structure factors and both types of interaction. In each case the Δ_k's for $K_A\leqslant k\leqslant K_W$ exhibit a pseudoasymptotic behavior. In panel (a) it starts at $K_A=2$, in panel (b) at $K_A=3$, and in panels (c) and (d) at $K_A=1$. The number K_W marks the beginning of the crossover from zero growth to power-law growth, which is most conspicuously observable in panel (d). K_W becomes smaller with increasing coupling strength. When we have $K_W\simeq K_A$, we are in the strong-coupling regime.[19]

In the weak-coupling regime, the systematic deviations from Eq. (3.10) are of two kinds: (i) The Δ_k sequence tends to converge toward a higher or lower value $\Delta_\infty^{(W)}$ as k increases toward K_W. (ii) The Δ_{2k} and the Δ_{2k-1} approach the pseudoasymptotic value $\Delta_\infty^{(W)}$ from opposite sides. In Fig. 2 we observe that the direction of the shift, which changes with

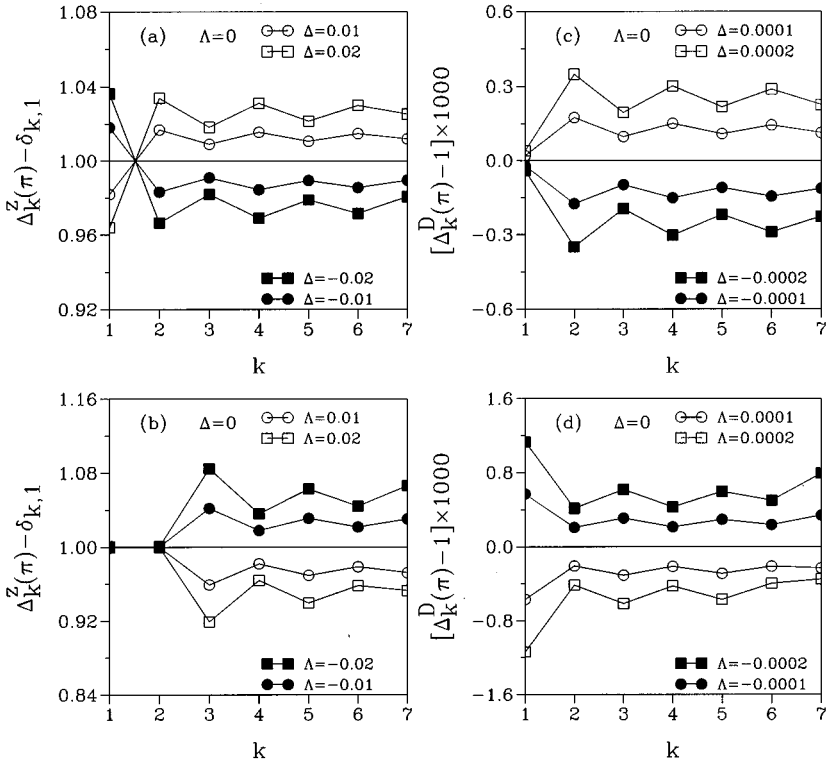

FIG. 2. Continued-fraction coefficients for the dynamic structure factors $S_{zz}(\pi,\omega)$ (left) and $S_{DD}(\pi,\omega)$ (right) at $T=0$ in the weak-coupling regime of Hamiltonian (1.1) with $\Lambda=0$ (top) or $\Delta=0$ (bottom). The energy unit is $J_\perp=1$. These coefficients have been produced by the recursion algorithm (Ref. 17) applied to the wave function $S^z_\pi|\Phi\rangle$ (left) or $D_\pi|\Phi\rangle$ (right), where $|\Phi\rangle$ is the finite-N ground-state wave function.

the sign of either interaction, is the same for both dynamic structure factors but opposite for the two types of coupling, whereas the alternating pattern, which also changes with the sign of either interaction, has the same direction for both functions and for both types of coupling.

For a quantitative analysis of the two pseudoasymptotic effects we must select the string of Δ_k's carefully. In $S_{DD}(\pi,\omega)$, the value K_W is considerably smaller than in $S_{zz}(\pi,\omega)$ for a given coupling strength, which restricts the weak-coupling analysis of $S_{DD}(\pi,\omega)$ to a narrower range of couplings.

The shift of the pseudoasymptotic value $\Delta_\infty^{(W)}$ [effect (i)] describes the renormalized bandwidth ω_0 of the dynamically predominant two-particle continuum of lattice fermions via the relation[17]

$$\Delta_\infty^{(W)}=\omega_0^2/4. \tag{3.11}$$

For pure NN coupling ($\Lambda=0$, $|\Delta|<0.1$), the band-edge frequency ω_0 inferred from the average of $\Delta_2,\ldots,\Delta_5$ was shown to reproduce the exact bandwidth $\epsilon_U(\pi)=2J_\Delta$ of the spinon continuum (3.3) very accurately.[19]

The alternating approach of the Δ_k's toward $\Delta_\infty^{(W)}$ [effect (ii)] describes an infrared singularity (3.6) in the two dynamic structure factors. For a truly convergent Δ_k sequence, the singularity exponent β is governed by the leading term of the large-k asymptotic expansion:[17,25]

$$\Delta_k=\Delta_\infty\left[1-(-1)^k\frac{\beta}{k}+\cdots\right]. \tag{3.12}$$

In Ref. 19 we proposed and tested two procedures (*averaging* and *extrapolation*) for extracting the exponent from a finite Δ_k sequence. For the NN case ($\Lambda=0$, $|\Delta|\leqslant 0.05$), a benchmark test showed that the exponent β_z inferred from the coefficients $\Delta_2,\ldots,\Delta_5$ reproduces [via Eq. (3.7)] the exact correlation function exponent (3.5) with reasonable accuracy.

The patterns in Fig. 2 make it clear that in the (Δ,Λ) plane there are sectors with compressed ($\Delta\omega_0<0$) and expanded ($\Delta\omega_0>0$) bandwidth, and sectors with divergent ($\beta<0$) and cusp ($\beta>0$) singularities. We have determined these boundaries between the resulting four sectors near the free-fermion point ($\Delta=0$, $\Lambda=0$) by a systematic investigation of the Δ_k sequences along several lines in parameter space.

One such series of sequences for $S_{zz}(\pi,\omega)$ is displayed in Fig. 3. Between $\Delta=-0.005$ (bottom sequence) and $\Delta=0.006$ (top sequence) at fixed $\Lambda=-0.001$, we observe a gradual reversal of both patterns (i) and (ii). At $\Delta\simeq-0.002$, the average Δ_k goes from negative to positive, implying a corresponding change in sign of $\Delta\omega_0^z$. At $\Delta\simeq 0.002$, the average of $\Delta_{2k-1}-\Delta_{2k}$ goes from positive to negative, implying a corresponding change in sign of the infrared exponent β_z. The two sequences closest to the pattern changes are highlighted by full symbols.

The lines in parameter space on which the interaction leaves the bandwidth ω_0^z or the exponent β_z unchanged depend somewhat on the Δ_k strings used for the analysis. This is illustrated in Fig. 4. The expectation is that the results improve as we shift the Δ_k string to higher indices k, where nonasymptotic effects become weaker.[26] Our best results, inferred from the string $\Delta_4,\ldots,\Delta_7$, yield sector boundaries at coupling ratios $\Delta/\Lambda\simeq 0.52$ for $\Delta\omega_0^z=0$ and $\Delta/\Lambda\simeq-0.44$ for $\beta_z=0$, in fair agreement with the corresponding sector boundaries $\Delta/\Lambda=0.5$ for $\Delta v_s=0$ and $\Delta/\Lambda=-0.5$ for $\Delta\eta_z=0$, respectively, predicted by the continuum results (3.8) and (3.4) and shown as long-dashed lines in Fig. 4.

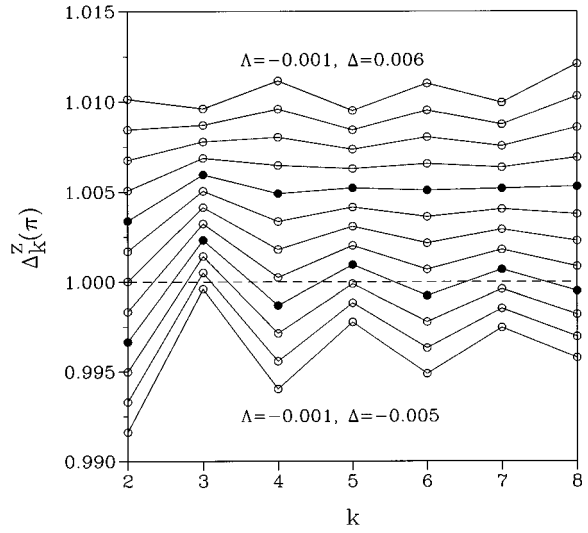

FIG. 3. Δ_k sequences for the dynamic spin structure factor $S_{zz}(\pi,\omega)$ at $\Lambda=-0.001$, $\Delta=-0.005,-0.004,\ldots,0.006$ as produced by the recursion algorithm (Ref. 17). The energy unit is $J_\perp=1$. The sequences for $\Delta=\pm0.002$ are marked by solid symbols.

C. Infrared exponent and bandwidth

Figure 5(a) shows the weak-coupling continued-fraction results for the infrared exponent $\beta_z(\Delta,\Lambda)$ at coupling strengths along the circle

$$\Delta=\Gamma\cos\theta,\quad \Lambda=\Gamma\sin\theta, \tag{3.13}$$

with radius $\Gamma=0.01$ around the free-fermion point in the (Δ,Λ) plane. The three data sets from different Δ_k strings[27]

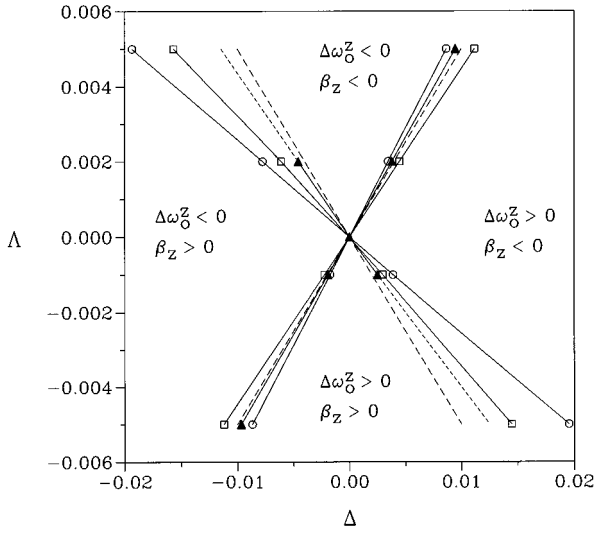

FIG. 4. The spin-fluid phase in the weak-coupling regime is divided into four sectors with infrared exponents β_z and bandwidth renormalization $\Delta\omega_0^z$ of opposite sign. The solid lines denote the sector boundaries derived from the strings $\Delta_2,\ldots,\Delta_5$ (circles), $\Delta_3,\ldots,\Delta_6$ (squares), and $\Delta_4,\ldots,\Delta_7$ (triangles). One solid line is extended short-dashed into the weak–strong-coupling crossover region of coefficient Δ_7. The long-dashed lines with slope $\Lambda/\Delta=\pm1/2$ are the sector boundaries predicted by the continuum analysis.

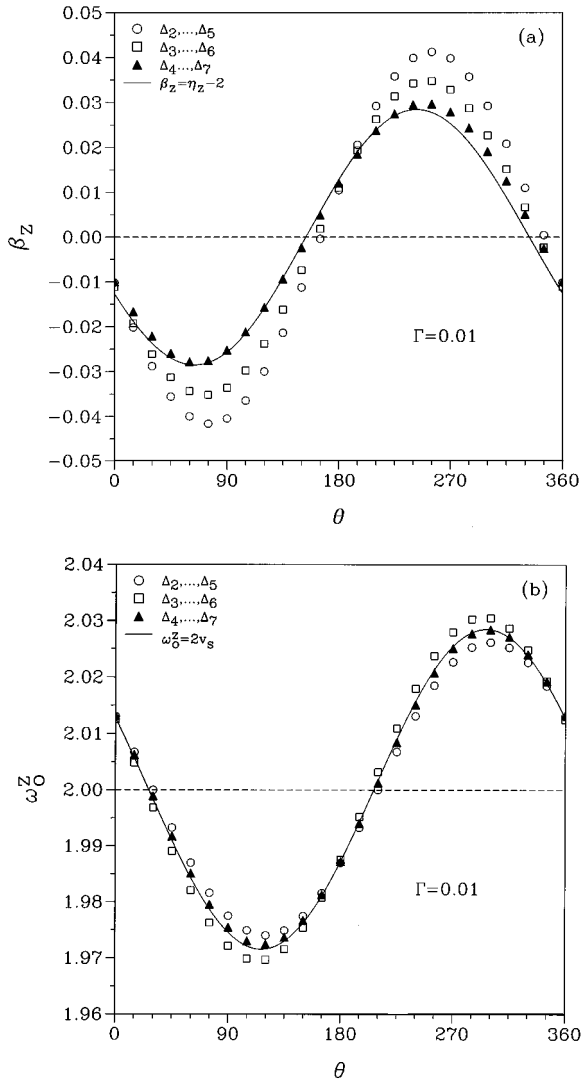

FIG. 5. (a) Infrared exponent β_z of $S_{zz}(\pi,\omega)$ and (b) renormalized bandwidth ω_0^z of the two-spinon continuum at different coupling ratios $\Lambda/\Delta=\tan\theta$ and fixed coupling strength $\sqrt{\Delta^2+\Lambda^2}=\Gamma=0.01$. The squares, circles, and triangles represent the results of a weak-coupling continued-fraction analysis based on three different Δ_k strings. The solid lines in (a) and (b) are derived from the continuum results (3.4) and (3.8), respectively. The energy unit is $J_\perp=1$.

fall onto sinelike curves in this representation, as does the prediction inferred from the continuum result (3.4), shown here as a solid line.

The best overall agreement between our data and Haldane's result occurs at angles $\theta\simeq9.5°,189.5°$, which correspond to the special coupling ratio $\Lambda/\Delta=1/6$ with vanishing umklapp terms in the continuum Hamiltonian. However, the agreement between the dashed line and the data set from $\Delta_4,\ldots,\Delta_7$, which is least affected by nonasymptotic coefficients, is remarkably good at all angles.

The dependence of the renormalized bandwidth ω_0^z on the same angular variable θ is shown in Fig. 5(b) in a comparative plot of three sets of weak-coupling continued-fraction data and the prediction inferred via Eq. (3.9) from the continuum result (3.8) for the renormalized spin velocity. Again

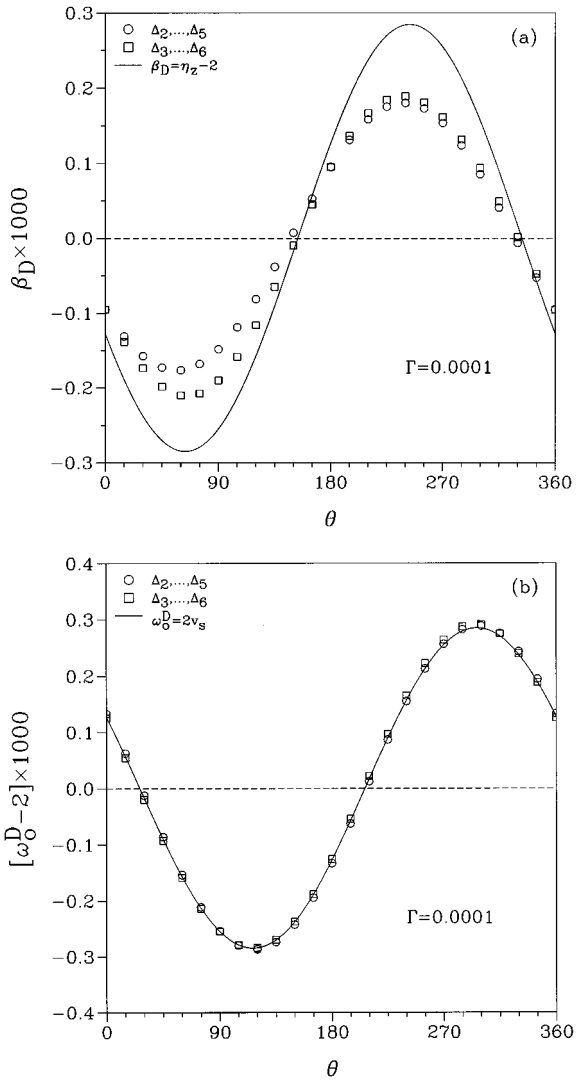

FIG. 6. (a) Infrared exponent β_D of $S_{DD}(\pi,\omega)$ and (b) renormalized bandwidth ω_0^D of the two-spinon continuum at different coupling ratios $\Lambda/\Delta=\tan\theta$ and fixed coupling strength $\sqrt{\Delta^2+\Lambda^2}=\Gamma=0.0001$. The squares and circles represent the results of a weak-coupling continued-fraction analysis based on two different Δ_k strings. The solid lines in (a) and (b) are derived from the continuum results (3.4) and (3.8), respectively. The energy unit is $J_\perp=1$.

the agreement improves as the Δ_k string is shifted toward higher indices, where it is less affected by nonasymptotic coefficients.

When the exponent and bandwidth are determined for a circle of much smaller radius, $\Gamma=0.0001$, we find the same angular dependence of β_z and ω_0^z and the same (rescaled) amplitude within a 5% margin of error. This confirms that the Δ_k's used in this analysis are free of weak–strong-coupling crossover effects.

We have carried out the same analysis for the renormalized bandwidth ω_0^D and the infrared exponent β_D of $S_{DD}(q,\omega)$. The results for parameter values on a circular line with radius $\Gamma=0.0001$ are displayed in Fig. 6. This radius had to be chosen much smaller than in the case of $S_{zz}(\pi,\omega)$ in order to ascertain that at least the coefficients $\Delta_2,\ldots,\Delta_6$ are free of crossover effects.

The bandwidth data from two different Δ_k strings depicted in Fig. 6(b) are in near perfect agreement with each other and with the result inferred from Eq. (3.8). Likewise the data for the exponent β_D as shown in Fig. 6(a) exhibit the same characteristic oscillation as already observed in Fig. 5(a) for β_z. The phase of the oscillation predicted by Eq. (3.4) is accurately reproduced by our data. There are significant deviations in the amplitude, which are attributable to the strongly nonasymptotic nature of the coefficients Δ_2,Δ_3, but the trends indicated by the two data sets are in the right direction.

The angular dependences of the exponent and bandwidth data shown in Figs. 5 and 6 are observed to be out of phase by some 55°, giving rise to the four sectors of weak-coupling dynamical behavior discussed in the context of Fig. 4. This is consistent with Haldane's predictions (3.4) and (3.8) for the correlation exponent and the renormalized Fermi velocity, respectively. These quantities have extreme values at $\tan\theta=2$ and $\tan\theta=-2$, respectively, which correspond to angles $63.4°$ and $116.6°=63.4°+53.2°$.

The characteristic oscillations of the infrared-exponent data are also expected to be present (with the same phase) in the angular dependence of the static spin and dimer structure factors at the critical wave number $q=\pi$. In the free-fermion limit, the Fourier transform of the exact results (2.5) and (2.6) yields

$$S_{zz}(q)=\frac{|q|}{2\pi},\quad S_{DD}(q)=\frac{1}{\pi}[|q|-|\sin q|]. \tag{3.14}$$

Both functions have a cusplike maximum at $q=\pi$, which reflects the critical spin and dimer fluctuations, respectively, in the ground state. It is reasonable to expect that the variation of $S_{zz}(\pi)$ and $S_{DD}(\pi)$ with the interaction in the weak-coupling limit is synchronized with the variation of the correlation exponent $\eta_z=\eta_D$ and, hence, with the infrared exponent $\beta_z=\beta_D$.

In Fig. 7 we have plotted the θ dependence of $S_{zz}(\pi)$ and $S_{DD}(\pi)$ for fixed coupling strengths $\Gamma=0.0001$. Both quantities exhibit the characteristic sinusoidal behavior. The amplitude is proportional to Γ in each quantity. Interestingly, the phases are different. Whereas $S_{DD}(\pi)$ varies in phase with the infrared exponent, $S_{zz}(\pi)$ does not.

D. Reconstruction of $S_{zz}(\pi,\omega)$ and $S_{DD}(\pi,\omega)$

The third major feature (in addition to the renormalized bandwidth and the infrared exponent) characterizing the line shape of the dynamic spin and dimer structure factors at the critical wave number $q=\pi$ is the detailed spectral-weight distribution near the band edge. For the pure NN case ($\Lambda=0$), we found that $\Delta\neq0$ causes a redistribution of the spectral weight in $S_{zz}(\pi,\omega)$ near the band edge and (for $\Delta<0$ only) the appearance of a discrete spectral line outside the band.[19] This discrete state was identified (by Bethe ansatz) to belong to a branch of bound spin complexes.

For the more general model (1.1) with $\Lambda\neq0$, it is not known for which parameter values such discrete states exist. We have investigated this question for parameter values (Δ,Λ) on the circular line (3.13) by means of a weak-coupling continued-fraction reconstruction of $S_{zz}(\pi,\omega)$

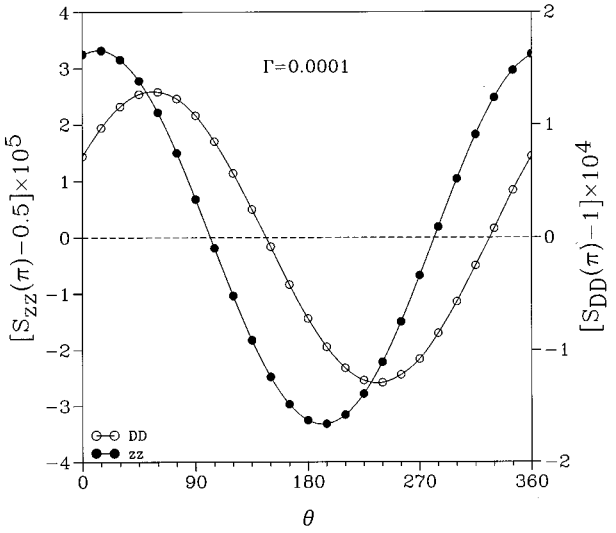

FIG. 7. Integrated intensities $S_{zz}(\pi)$ and $S_{DD}(\pi)$ of the spin and dimer order-parameter fluctuations, respectively, at different coupling ratios $\Lambda/\Delta=\tan\theta$ and fixed coupling strength $\Gamma=\sqrt{\Delta^2+\Lambda^2}=0.0001$ as derived from the ground-state wave function for $N=16$.

based on the coefficients $\Delta_1,\ldots,\Delta_{K_w}$ and a termination function which incorporates the renormalized bandwidth ω_0^z and the infrared exponent β_z. A detailed description of the procedure can be found in Refs. 17 and 19.

The dependence on the angular parameter θ of the reconstructed $S_{zz}(\pi,\omega)$ is displayed in Fig. 8. As θ increases from zero to 60° [panel (a)], the bandwidth shrinks and the infrared divergence gains strength. In addition to these two features we observe the emergence at $\theta\simeq 15°$ of a discrete spectral line above and outside the band. In the reconstructed relaxation function the discrete state is represented by an isolated pole. For $z=\epsilon-i\omega$ with $\epsilon=0.0001$ it has a nonzero width. At $\theta=15°$, the discrete state is barely distinguishable from the band edge.

Between $\theta=60°$ and $\theta=120°$ the bandwidth continues to shrink, while more and more spectral weight is transferred from the continuum to the discrete state. The infrared divergence, which has reached its maximum strength at $\theta\simeq 60°$, weakens over this parameter range. The further evolution of the line shapes near the band edge and at small frequencies is shown in panel (b). The infrared divergence disappears at $\theta\simeq 150°$ and turns into a cusp singularity (see inset). The bandwidth of the continuum expands while the discrete state moves closer to the band edge and slowly loses spectral weight.

These trends continue between $\theta=195°$ and $\theta=240°$ as shown in panel (c). The depletion of spectral weight at small ω becomes more and more prounouced, and the discrete state merges with the band edge at $\theta\simeq 210°$. Nothing dramatic happens to the line shape on the last stretch of the circle. The range of parameter values where a discrete state is observed, $30°\leqslant\theta\leqslant 210°$, roughly coincides with the range where the renormalized bandwidth is compressed. In the fermion representation, this is the region, where the Fermi velocity is renormalized downward.

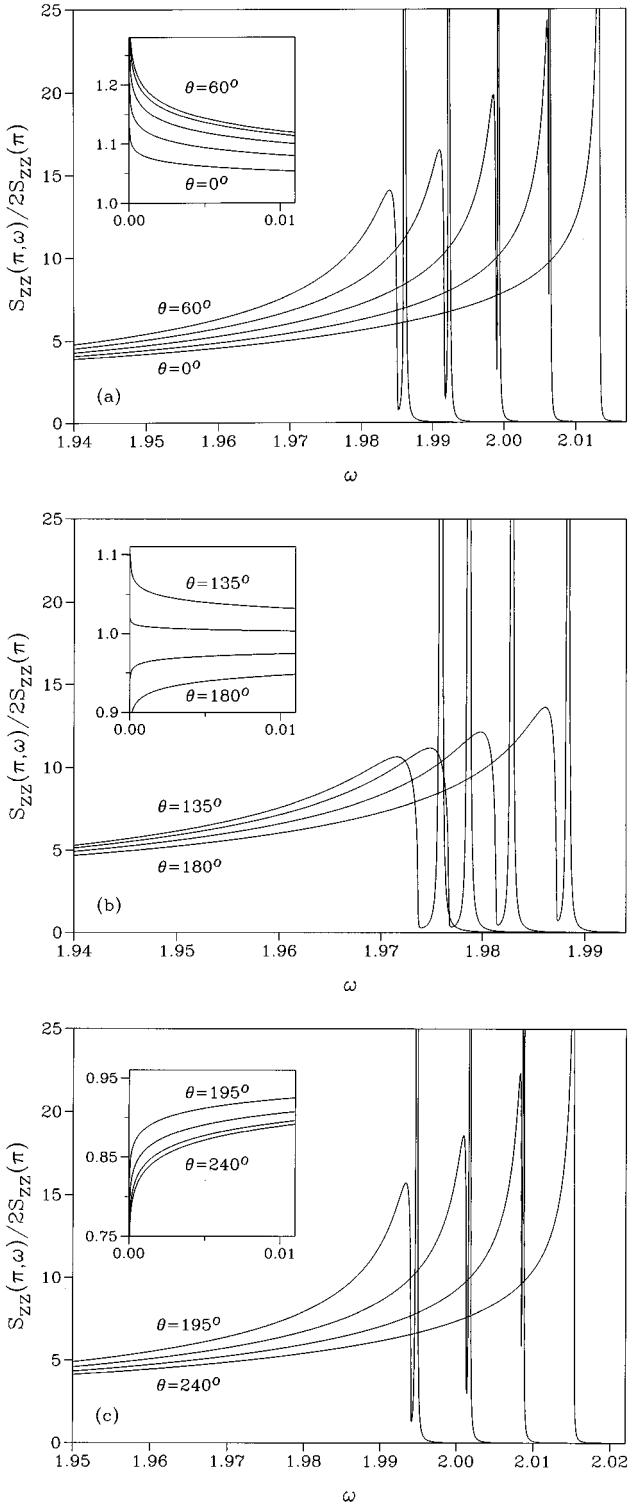

FIG. 8. Dynamic spin structure factor $S_{zz}(\pi,\omega)$ at different coupling ratios $\Lambda/\Delta=\tan\theta$ and fixed coupling strength $\sqrt{\Delta^2+\Lambda^2}=\Gamma=0.01$, specifically for the angles (a) $\theta=0°,15°,\ldots,60°$, (b) $\theta=135°,150°,\ldots,180°$, and (c) 195°,210°, . . . ,240°. The main plot depicts the line shapes near the band edge and the inset the line shapes at low frequencies. All curves have resulted from a weak-coupling continued-fraction reconstruction based on the coefficients $\Delta_1,\ldots,\Delta_7$ and a compact α terminator as explained in Refs. 17 and 19. The energy unit is $J_\perp=1$.

In the weak-coupling reconstruction of $S_{DD}(\pi,\omega)$, which starts from the expression (3.2) and the constant Δ_k sequence (3.10), the effects of a weak interaction (3.13) on the line shape are similar in two aspects yet different in a third aspect. (i) The low-frequency behavior is governed by a weak infrared singularity which switches from a divergence to a cusp in accordance with the exponent data presented in Fig. 6(a). (ii) The only noticeable change at the band edge is the variation of the continuum boundary in accordance with the bandwidth data presented in Fig. 6(b). (iii) However, no noticeable rearrangement of spectral weight near the band edge occurs unlike what has been observed in $S_{zz}(\pi,\omega)$. In particular, the discrete state found in $S_{zz}(\pi,\omega)$ does not carry any spectral weight in $S_{DD}(\pi,\omega)$. It does not play any role in the dimer fluctuations.

ACKNOWLEDGMENTS

The work at URI was supported by the U.S. National Science Foundation, Grant No. DMR-93-12252, and the work at ORNL by the U.S. Department of Energy under Contract No. DE-FG06-94ER45519. Computations were carried out at the National Center for Supercomputing Applications, University of Illinois at Urbana-Champaign.

[1] A recent study with many references to earlier work is the following: J. Richter, Phys. Rev. B **47**, 5794 (1993).
[2] C. K. Majumdar and D. K. Ghosh, J. Math. Phys. **10**, 1388 (1969).
[3] P. M. Van den Broek, Phys. Lett. **77A**, 261 (1980).
[4] B. S. Shastry and B. Sutherland, Phys. Rev. Lett. **47**, 964 (1981).
[5] F. D. M. Haldane, Phys. Rev. B **25**, 4925 (1982); **26**, 5257 (1982).
[6] T. Tonegawa and I. Harada, J. Phys. Soc. Jpn. **56**, 2153 (1987).
[7] M. Schmidt, C. Gerhardt, K.-H. Mütter, and M Karbach, J. Phys. Condens. Matter **8**, 553 (1996).
[8] E. Lieb, T. Schultz, and D. Mattis, Ann. Phys. (N.Y.) **16**, 407 (1961).
[9] S. Katsura, Phys. Rev. **127**, 1508 (1962).
[10] H. P. Bader and R. Schilling, Phys. Rev. B **19**, 3556 (1979).
[11] Y. Yu and G. Müller, J. Appl. Phys. **79**, 4629 (1996).
[12] Y. Yu, M. Karbach, and G. Müller (unpublished).
[13] R. Haydock, Solid State Phys. **35**, 215 (1980).
[14] *The Recursion Method and its Applications,* edited by D. G. Pettifor and D. L. Weaire (Springer-Verlag, New York, 1985).
[15] M. H. Lee, Phys. Rev. B **26**, 2547 (1982).
[16] E. R. Gagliano and C. A. Balseiro, Phys. Rev. B **38**, 11 766 (1988).
[17] V. S. Viswanath and G. Müller, *The Recursion Method: Application to many-body dynamics*, Lecture Notes in Physics Vol. m23 (Springer-Verlag, New York, 1994).
[18] V. S. Viswanath, S. Zhang, J. Stolze, and G. Müller, Phys. Rev. B **49**, 9702 (1994).
[19] V. S. Viswanath, S. Zhang, G. Müller, and J. Stolze, Phys. Rev. B **51**, 368 (1995).
[20] Th. Niemeijer, Physica **36**, 377 (1967).
[21] S. Katsura, T. Horiguchi, and M. Suzuki, Physica **46**, 67 (1970).
[22] B. M. McCoy, E. Barouch, and D. B. Abraham, Phys. Rev. A **4**, 2331 (1971); B. M. McCoy, J. H. H. Perk, and R. E. Shrock, Nucl. Phys. **220** [FS8], 35 (1983); **220** [FS8], 269 (1983); G. Müller and R. E. Shrock, Phys. Rev. B **29**, 288 (1984).
[23] G. Müller, H. Thomas, H. Beck, and J. C. Bonner, Phys. Rev. B **24**, 1429 (1981).
[24] A. Luther and I. Peschel, Phys. Rev. B **12**, 3908, (1975).
[25] A. Magnus, in *The Rescursion Method and its Applications* (Ref. 14), p. 22.
[26] Obviously, the weak-coupling continued-fraction results for the infrared exponent β_z and the renormalized bandwidth ω_0 from a string $\Delta_{k_i},\ldots,\Delta_{k_f}$ of coefficients are vulnerable to systematic errors. The two main sources of systematic error are the following: (i) If k_i is chosen too small ($k_i<K_A$), then the first one or several Δ_k's are too strongly nonasymptotic in character and introduce a bias into the pseudoasymptotic analysis. (ii) If k_f is chosen too high ($k_f>K_W$), then the last one or several Δ_k's are affected by the crossover to nonzero growth rate, which introduces a different kind of bias.
[27] In Ref. 19 we showed that the accuracy of the weak-coupling continued-fraction results for the case $\Lambda=0$ can yet be improved substantially if we use *extrapolation* instead of *averaging*. However, since the data do not lend themselves to extrapolation for all coupling ratios, we employ the more robust averaging method for all cases here.